Theory and Experiment of the Hemispherical Cavity-Backed Slot Antenna

K. W. Leung, *Member, IEEE* and K. Y. Chow

***Abstract*— The hemispherical cavity-backed slot antenna is studied theoretically and experimentally. The exact magnetic field Green's function of the cavity is derived rigorously and expressed in a form convenient for numerical computation. The moment method is used to find the equivalent magnetic current in the slot and, hence, the input impedance of the antenna configuration. The effects of the cavity size, of the slot length, and of the slot offset on the input impedance are studied and very good agreement between theory and experiment is obtained. The variation of the magnetic current around the slot and cavity resonances are discussed. Comparisons between the rigorous solution and the single-mode theory are given and the limitation of the single-mode theory is discussed.**

I. Introduction

THE SLOT antenna has been an important subject for many years. It offers several advantages such as low profile, light weight, easy fabrication, and high-power capability. These features make the slot antenna very suitable for airborne applications. An open slot antenna cut in an infinite ground plane has the simplest structure and is easy to analyze via the Booker relationship [1]. However, the open slot antenna radiates equally from both sides and, thus, limits the application. A remedy to the problem is to cover the back of the slot by a metallic cavity, the so-called cavity-backed slot antenna [2]–[8]. By using the cavity, the radiation of the antenna is restricted to the front side only and the radiation efficiency on the side is increased. Moreover, as the cavity-backed slot antenna has relatively weak mutual coupling in the array configuration, it is a suitable candidate for a large antenna-array system.

Owing to the presence of the cavity, the symmetry upon which the Booker relationship depends is destroyed and the analysis becomes more complicated. Cockrell [2] employed the complex Poynting theorem to calculate the input admittance of the rectangular cavity-backed slot antenna. He calculated the input admittance by separating the electromagnetic fields into parts external and internal to the cavity. While the external part had been studied in [9], the internal part was obtained by expanding the cavity's field in modes of an ideal hollow waveguide. The waveguide was then shorted by a conducting plane at one end and by a conducting plane containing the slot at the other end. Finally, the two parts of the solution were combined by equating the input power to the power entering the cavity plus that radiating into the half-space. In this method, a single piecewise sinusoidal (PWS) term was used to model the aperture field. Such an assumption is justified only at relatively low frequencies and is not valid in general. Galejs [3] and Hadidi and Hamid [4] used the Green's function technique to find the input admittance/impedance of the rectangular cavity-back slot antenna. Instead of considering the conservation of the complex power, they enforced the boundary condition of the magnetic field across the slot and formulated an integral equation for the unknown magnetic current (or aperture field) in the slot. The magnetic current and, hence, the input admittance/impedance, were then found using the variational method [3] or the moment method (MoM) [4]. This approach is more flexible than the previous one in that the accuracy of the magnetic current can be improved by adding more basis (trial) functions. Of course, when a delta-gap source is used to model the excitation, the number of basis function cannot be too large or a divergent solution results [10], [11]. Apart from the rigorous theory, Long [5] carried out extensive measurements from which a mathematical model was derived [6].

The cavity has long been concentrated on the rectangular shape [2]–[7]. Recently, Li *et al.* [8] studied the cylindrical version. They calculated the input impedance using the complex Poynting theorem and verified the results by experiment. Lately, a new configuration, the hemispherical cavity-backed slot antenna, was considered for the cavity TE_{111} mode [12] using the single-mode theory [13]–[16]. In this paper, the hemispherical cavity-backed slot antenna is analyzed rigorously and verified by measurements. The Green's function approach [3]–[4] is used to formulate the problem, which is solved using MoM. The Green's function for the upper half-space has been well studied and will not be discussed in detail. For the cavity part, the mode-matching method [17] is used to derive the magnetic field Green's function rigorously. To enhance the numerical efficiency, the modal solution of the Green's function is represented as a sum of the particular and homogeneous solutions [18]. Physically, the particular solution accounts for the source radiating in an unbounded medium, whereas the homogeneous solution for the boundary discontinuity. We will use the physical argument to solve the problem arising from the slowly convergent particular solution [17]. Consequently, the modal solution converges very quickly, making the computation very fast. In this paper, the results using the rigorous solution will be compared with those using the single-mode approximation [12] and the limitation of the single-mode theory is discussed.

Manuscript received July 30, 1996; revised May 29, 1998. This work is supported by the City University of Hong Kong Project 7000496 under Strategic Research Grant and the RGC Earmarked Research Grant Project 9040209.

The authors are with the Department of Electronic Engineering, City University of Hong Kong, Kowloon, Hong Kong.

Publisher Item Identifier S 0018-926X(98)06108-0.

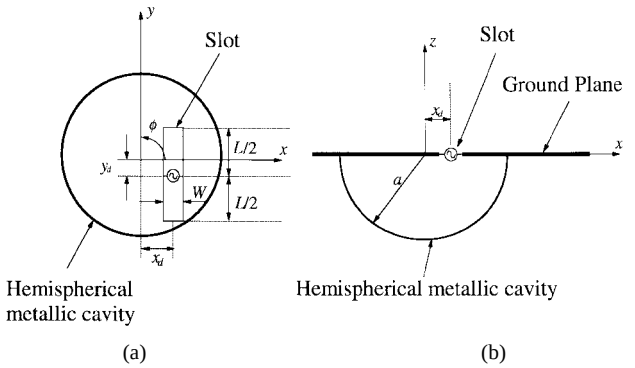

Fig. 1. The geometry of the hemispherical cavity-backed slot antenna. (a) Top view. (b) Side view.

Furthermore, the effects of the cavity size, of the slot length, and of the slot offset on the input impedance are investigated. While studies of the cavity-backed slot antenna were usually concentrated on the slot resonance, some discussions on the cavity resonance are also addressed in this paper. The first few fundamental cavity TM and TE modes are considered and their excitations discussed. Finally, we will discuss the variation of the magnetic current around the slot resonance as well as the cavity resonance.

II. Formulation

The geometry of the hemispherical cavity-backed slot antenna is shown in Fig. 1, where the slot of length L and of width W is cut from an infinite ground plane. Beneath the slot is a hemispherical cavity of radius a. The slot has offsets x_d and y_d from the y axis and x axis, respectively. In the following formulation, the fields are assumed to vary harmonically as $e^{j\omega t}$, which is suppressed. Furthermore, $\vec{r}(x,y,z)$ and $\vec{r}'(x',y',z')$ refer to the field and source points, respectively. Since only the slender slot $(k_0 W \ll 1, W \ll L)$ is considered in this paper, we assume that the equivalent magnetic current M_y in the slot is a function of y only and excited at $y = y_0$. To begin with, we enforce the boundary condition of the magnetic field across the slot $(z = 0)$

$$H_y^u - \left(-H_y^c\right) = I_0 \delta(y - y_0) \tag{1}$$

where the superscripts u and c denote the fields on the upper half plane and inside the cavity, respectively, and I_0 is the terminal current of the excitation source. We then invoke image theory so that the free-space and the spherical cavity, instead of the half-space and the hemispherical cavity, are considered. It follows from (1) that

$$\iint_{S_0} [G_f(x,y;x',y') + G_c(x,y;x',y')][-2M_y(y')]\, dS' = I_0 \delta(y - y_0) \tag{2}$$

where G_f and G_c are the free-space and spherical-cavity Green's functions, respectively, and S_0 is the surface of the slot. In (2), M_y has been multiplied by "-2," where the factor of two accounts for the effect of the ground plane and the minus sign ensures that the tangential field is equal on each side of the slot region.

Let

$$K_y(y) = M_y(y) W \tag{3}$$

and expand K_y by a set of basis function $f_n(y)$

$$K_y(y) = \sum_{n=1}^{N} V_n f_n(y) \tag{4}$$

where V_n's are unknown coefficients to be determined. Then, by inserting (3) and (4) into (2) and setting I_0 to unity for convenience, one obtains

$$\frac{-2}{W^2} \sum_{n=1}^{N} V_n \iint_{S_0} [G_f(x,y;x',y') + G_c(x,y;x',y')] f_n(y')\, dS' = \delta(y - y_0). \tag{5}$$

Using the Galerkin's procedure the following matrix equation is obtained:

$$[Y_{mn}][V_n] = \left[\frac{1}{2} f_m(y_0)\right], \qquad n,m = 1,2,\cdots,N \tag{6}$$

where

$$Y_{mn} = Y_{mn}^f + Y_{mn}^c \tag{7}$$

$$Y_{mn}^\beta = \frac{-1}{W^2} \iint_{S_0} \iint_{S_0} f_m(y) G_\beta(x,y;x',y') f_n(y')\, dS'\, dS \tag{8}$$

and $\beta = f$ or c. To solve for the matrix $[V_n]$, it is required to calculate the slot admittance $Y_{mn} = Y_{mn}^f + Y_{mn}^c$. First, we evaluate the free-space admittance Y_{mn}^f. It involves the Green's function G_f which has been well studied and given by

$$G_f = \frac{-j}{\omega \mu_0} \left(\frac{\partial^2}{\partial y^2} + k_0\right) \frac{e^{-jk_0 R}}{4\pi R} \tag{9}$$

where $R = \sqrt{(x-x')^2 + (y-y')^2}$ is the distance between the field and source points on the ground plane $(z = z' = 0)$. Since Y_{mn}^f simply represent the self and mutual admittances, which are coordinate independent, we will calculate Y_{mn}^f as if the slot were located at the center of the coordinate system. Then by using the equivalent radius $a_e = W/4$ [19], the admittance Y_{mn}^f can be easily found from the knowledge of the cylindrical dipole. Note that G_f has a singularity occurring at $\vec{r} = \vec{r}'$, causing a numerical problem in performing the numerical integration. To avoid this difficulty, the distance R is replaced by $R' = \sqrt{(y-y')^2 + a_e^2}$ and the resulting Green's function is the so-called "reduced kernel." In this case, Y_{mn}^f can be written in the Richmond form [20], which can be implemented numerically in a straightforward manner. In the next section, we will derive the cavity Green's function G_c rigorously from which the cavity admittance Y_{mn}^c is found.

III. Derivation of the Cavity Green's Function G_c

To begin with, image theory is used so that an equivalent problem of a magnetic current flowing inside a spherical cavity is obtained. To comply with the geometry of the cavity, the magnetic current M_y on the ground plane ($z' = 0$ or $\theta' = \pi/2$) is first decomposed into its spherical components $M_r = M_y \sin\phi'$ and $M_\phi = M_y \cos\phi'$. Since M_ϕ can excite TE to r and TM to r modes, both the electric potential function $G^{F_r}_{M_\phi}$ and the magnetic potential function $G^{A_r}_{M_\phi}$ are required to represent all possible fields it excites. On the other hand, however, one electric potential function $G^{F_r}_{M_r}$ alone is sufficient for the M_r case as M_r can excite TE to r modes only. Note that when the slot is aligned with the $\hat{y}$ axis (a diameter), we have $\phi' = \pi/2$ or $3\pi/2$ so that $M_\phi = 0$ and only M_r remains. In the following derivation, we use the letters p and h to denote the particular and homogeneous solutions, respectively.

A. Green's Functions $G^{F_r}_{M_\phi}$ and $G^{A_r}_{M_\phi}$

Particular Solutions

$$G^{F_{rp}}_{M_\phi} = \sum_{n=0}^{\infty}\sum_{m=-n}^{n} A_{nm} P_n^m(\cos\theta) e^{jm\phi} \Phi_n'(k_0 r') \Psi_n(k_0 r) \tag{10}$$

$$G^{A_{rp}}_{M_\phi} = \sum_{n=0}^{\infty}\sum_{m=-n}^{n} D_{nm} P_n^m(\cos\theta) e^{jm\phi} \Phi_n(k_0 r') \Psi_n(k_0 r) \tag{11}$$

where

$$\Phi_n(k_0 r') = \begin{cases} \hat{J}_n(k_0 r'), & r > r' \\ \hat{H}_n^{(2)}(k_0 r'), & r < r' \end{cases} \tag{12}$$

$$\Psi_n(k_0 r) = \begin{cases} \hat{H}_n^{(2)}(k_0 r), & r > r' \\ \hat{J}_n(k_0 r), & r < r' \end{cases} \tag{13}$$

Homogeneous Solutions

$$G^{F_{rh}}_{M_\phi} = \sum_{n=0}^{\infty}\sum_{m=-n}^{n} B_{nm} P_n^m(\cos\theta) e^{jm\phi} \hat{J}_n(k_0 r) \tag{14}$$

$$G^{A_{rh}}_{M_\phi} = \sum_{n=0}^{\infty}\sum_{m=-n}^{n} E_{nm} P_n^m(\cos\theta) e^{jm\phi} \hat{J}_n(k_0 r) \tag{15}$$

In (10)–(15), $P_n^m(x)$ is the associated Legendre function of the first kind with order m and degree n and $\hat{J}_n(x)$ and $\hat{H}_n^{(2)}(x)$ are the spherical Bessel function of the first kind and the spherical Hankel function of the second kind, respectively. Both of them are of order n and of Schelkunoff type [21, p. 268]. All other symbols have the usual meanings. The unknown modal coefficients A_{nm} and D_{nm} are determined from the boundary conditions at the source point $\vec{r} = \vec{r}'$ (E_ϕ, H_θ and H_ϕ are continuous but E_θ is discontinuous by a surface magnetic current $M_{\phi s}$), whereas the modal coefficients B_{nm} and E_{nm} determined from the boundary condition at the cavity surface ($E_\theta = E_\phi = 0$ at $r = a$). Using the techniques of [17], the coefficients are obtained as follows:

$$G^{F_{rp}}_{M_\phi} = \frac{1}{r' \sin\theta'} \sum_{n=1}^{\infty}\sum_{m=1}^{n} a_{nm} P_n^m(\cos\theta') P_n^m \times (\cos\theta) \sin m(\phi - \phi') \Phi_n'(k_0 r') \Psi_n(k_0 r) \tag{16}$$

$$G^{A_{rp}}_{M_\phi} = \frac{1}{r'} \sum_{n=1}^{\infty}\sum_{m=0}^{n} d_{nm} \frac{dP_n^m(\cos\theta')}{d\theta'} P_n^m \times (\cos\theta) \cos m(\phi - \phi') \Phi_n(k_0 r') \Psi_n(k_0 r) \tag{17}$$

$$G^{F_{rh}}_{M_\phi} = \frac{1}{r' \sin\theta'} \sum_{n=1}^{\infty}\sum_{m=1}^{n} \alpha_n^{\mathrm{TE}} a_{nm} P_n^m(\cos\theta') P_n^m \times (\cos\theta) \sin m(\phi - \phi') \hat{J}_n'(k_0 r') \hat{J}_n(k_0 r) \tag{18}$$

$$G^{A_{rh}}_{M_\phi} = \frac{1}{r'} \sum_{n=1}^{\infty}\sum_{m=0}^{n} \alpha_n^{\mathrm{TM}} d_{nm} \frac{dP_n^m(\cos\theta')}{d\theta'} P_n^m \times (\cos\theta) \cos m(\phi - \phi') \hat{J}_n(k_0 r') \hat{J}_n(k_0 r) \tag{19}$$

where

$$a_{nm} = \frac{-j\varepsilon_0}{2\pi} \cdot \frac{2n+1}{n(n+1)} \cdot \frac{(n-m)!}{(n+m)!} \cdot m \tag{20}$$

$$d_{nm} = \frac{\omega\mu_0\varepsilon_0}{\Delta_m 2\pi k_0} \cdot \frac{2n+1}{n(n+1)} \cdot \frac{(n-m)!}{(n+m)!} \tag{21}$$

$$\Delta_m = \begin{cases} 1 & \text{for } m > 0 \\ 2 & \text{for } m = 0 \end{cases} \tag{22}$$

and $\alpha_n^{\mathrm{TE}} = -\hat{H}_n^{(2)}(k_0 a)/\hat{J}_n(k_0 a)$ and $\alpha_n^{\mathrm{TM}} = -\hat{H}_n^{(2)\prime}(k_0 a)/\hat{J}_n'(k_0 a)$ are the TE and TM modes reflection coefficients, respectively, at the cavity boundary. Note that if the cavity was not present, there was no reflected wave and, therefore, $\alpha_n^{\mathrm{TE}} = \alpha_n^{\mathrm{TM}} = 0$. In this case, the homogeneous solutions disappear and only the particular solutions remain, which is to be expected. It is interesting to note that when the denominators of α_n^{TE} and α_n^{TM} are set to zero, one obtains the characteristic equations of the TE and TM modes, respectively, as given in [21, pp. 269–271]. Finally the Green's functions $G^{F_r}_{M_\phi}$ and $G^{A_r}_{M_\phi}$ are given by

$$G^{F_r}_{M_\phi} = G^{F_{rp}}_{M_\phi} + G^{F_{rh}}_{M_\phi} \tag{23}$$

$$G^{A_r}_{M_\phi} = G^{A_{rp}}_{M_\phi} + G^{A_{rh}}_{M_\phi}. \tag{24}$$

B. Green's Function $G^{F_r}_{M_r}$

Following the procedure given in [21, pp. 267–269], one obtains the following differential equation for the particular solution $G^{F_{rp}}_{M_r}$ of $G^{F_r}_{M_r}$:

$$\left(\nabla^2 + k_0^2\right) \frac{G^{F_{rp}}_{M_r}}{r} = \frac{-\varepsilon_0}{r} \cdot \frac{\delta(r - r')\delta(\theta - \theta')\delta(\phi - \phi')}{r^2 \sin\theta}. \tag{25}$$

Equation (25) was solved [11] and the result is given by

$$G^{F_{rp}}_{M_r} = \frac{1}{r'^2} \sum_{n=0}^{\infty}\sum_{m=0}^{n} g_{nm} P_n^m(\cos\theta') P_n^m(\cos\theta) \times \cos m(\phi - \phi') \Phi_n(k_0 r') \Psi_n(k_0 r) \tag{26}$$

where

$$g_{nm} = \frac{-j\varepsilon_0}{2\pi\Delta_m k_0} \cdot \frac{(n-m)!}{(n+m)!} \cdot (2n+1). \tag{27}$$

By matching the boundary conditions on the cavity surface, the homogeneous solution is obtained as follows:

$$G_{M_r}^{F_{rh}} = \frac{1}{r'^2}\sum_{n=0}^{\infty}\sum_{m=0}^{n}\alpha_n^{\mathrm{TE}} g_{nm} P_n^m(\cos\theta')P_n^m(\cos\theta) \times \cos m(\phi-\phi')\hat{J}_n(k_0 r')\hat{J}_n(k_0 r). \quad (28)$$

Finally, the Green's function $G_{M_r}^{F_r}$ is given by

$$G_{M_r}^{F_r} = G_{M_r}^{F_{rp}} + G_{M_r}^{F_{rh}}. \quad (29)$$

C. Green's Function G_c

After the Green's functions $G_{M_r}^{F_r}$, $G_{M_\phi}^{F_r}$, and $G_{M_\phi}^{A_r}$ are found, the cavity Green's function G_c is obtained easily by following the procedure of [22]. It was found that the particular solution of G_c is a slowly convergent series of Hankel function. This causes a problem as the amplitudes of higher order Hankel functions are too large to handle numerically. To tackle the problem, recall that the particular solution simply represents a $\hat{y}$ directed magnetic field due to a $\hat{y}$ directed magnetic point current in an unbounded medium. This is exactly given by G_f, the free-space Green's function. Therefore, $G_c(z=z'=0$ or $\theta=\theta'=\pi/2)$ can be written as follows:

$$G_c = G_f + G_H \quad (30)$$

where

$$\begin{aligned} G_H = {} & \frac{-1}{4\pi\omega\mu_0 k_0}\cdot\frac{\sin\phi'\sin\phi}{r^2 r'^2}\sum_{n=1}^{\infty}\alpha_n^{\mathrm{TE}} n(n+1)(2n+1) \\ & \times P_n(\cos(\phi-\phi'))\hat{J}_n(k_0 r')\hat{J}_n(k_0 r) \\ & - \frac{1}{4\pi\omega\mu_0}\cdot\frac{\cos\phi'\sin\phi}{r^2 r'}\sum_{n=1}^{\infty}\alpha_n^{\mathrm{TE}}(2n+1) \\ & \times \frac{\partial P_n(\cos(\phi-\phi'))}{\partial\phi'}\hat{J}_n'(k_0 r')\hat{J}_n(k_0 r) \\ & - \frac{1}{4\pi\omega\mu_0}\cdot\frac{\sin\phi'\cos\phi}{r r'^2}\sum_{n=1}^{\infty}\alpha_n^{\mathrm{TE}}(2n+1) \\ & \times \frac{\partial P_n(\cos(\phi-\phi'))}{\partial\phi}\hat{J}_n(k_0 r')\hat{J}_n'(k_0 r) \\ & - \frac{\omega\varepsilon_0}{4\pi k_0}\cdot\frac{\cos\phi'\cos\phi}{r r'}\sum_{n=1}^{\infty}\alpha_n^{\mathrm{TM}}\frac{(2n+1)}{n(n+1)} \\ & \times P_n'(\cos(\phi-\phi'))\hat{J}_n(k_0 r')\hat{J}_n(k_0 r) \\ & - \frac{k_0}{4\pi\omega\mu_0}\cdot\frac{\cos\phi'\cos\phi}{r r'}\sum_{n=1}^{\infty}\alpha_n^{\mathrm{TE}}\frac{(2n+1)}{n(n+1)} \\ & \times \frac{\partial^2 P_n(\cos(\phi-\phi'))}{\partial\phi\partial\phi'}\hat{J}_n'(k_0 r')\hat{J}_n'(k_0 r) \end{aligned} \quad (31)$$

and G_f has been given in (9). Note that G_c is reciprocal in $\vec{r}$ and $\vec{r}'$, as expected. In deriving (31), the double-summations have been reduced to the single-summations by using the addition theorem for Legendre polynomials [21, p. 292]. In this paper, the rigorous solution will be compared with the single-mode theory [12].

IV. Evaluations of Y_{mn} and Input Impedance

From (7), (8), and (30), we have

$$Y_{mn} = 2Y_{mn}^f + Y_{mn}^H \quad (32)$$

where Y_{mn}^H is given by (8) with $\beta = H$. It was found that for the frequency range we are concerned with two basis functions of $f_1(y) = \sin k_0(L/2-|y|)$ and $f_2(y) = k_0(L/2-|y|)\cos k_0(L/2-|y|)$ are sufficient for the MoM convergence. It should be mentioned that for the particular choice of $f_1(y)$ and $f_2(y)$, one may calculate Y_{mn}^f by using the simple formula given in [23], which requires no numerical integrations at all. In addition, as the homogeneous solution G_H is a smooth and quickly convergent function, the computation of the input impedance is very efficient.

The input impedance of the cavity-backed slot antenna is given by

$$Z_{\mathrm{in}} = \frac{V_0}{I_0} = V_0 \quad (33)$$

where

$$V_0 = -\int_{x_d-W/2}^{x_d+W/2} E_x(x,y_0)\,dx = M_y(y_0)W \quad (34)$$

is the terminal voltage. From (3), (33), and (34), we have $Z_{\mathrm{in}} = K_y(y_0) = V_1 f_1(y_0) + V_2 f_2(y_0)$.

V. Measured and Computed Results

To verify the theory, measurements were carried out using the image technique [5], [8]. Three quarter-spherical cavities of radii $a = 6.25$, 7.28, and 8.73 cm were fabricated. The half-slot of width $W/2 = 1$ mm was cut in the edge of a thin copper plate. The edge is then butted up against an aluminum plate, which serves as an image plane. A coaxial probe of radius 0.63 mm was used to excite the half slot. The measurements were taken using an HP8510C network analyzer, with the reference plane set at the coaxial aperture using the port extension. By using the image technique, the measured input impedance is one-half of that of the original configuration (the whole slot without the image plane) [5], [8]. In this paper, the results are of the whole slot case.

The convergence of the modal Green's function G_H is first examined by varying the number of modal terms. It is worth mentioning that the number of modal term required for G_H to converge depends on the slot position. For example, when the slot is aligned with a cavity's diameter (e.g., $x_d = 0$), all TM modes cannot be excited because of lacking the M_ϕ component. Consequently, all TM modal terms can be neglected without affecting the accuracy of the solution. In particular, when the slot is located at the center of the cavity $(x_d = y_d = 0)$, not only all TM modes, but also some higher order TE modes are eliminated. When this happens, all TM modal terms together with the corresponding TE modal terms can be omitted in the numerical solution. Obviously, the solution G_H converges most quickly when $x_d = y_d = 0$ and the convergence is slowed down for other slot locations. It was found that the offset x_d has a stronger effect than y_d on the convergence, so to see the worst case the maximum x_d is

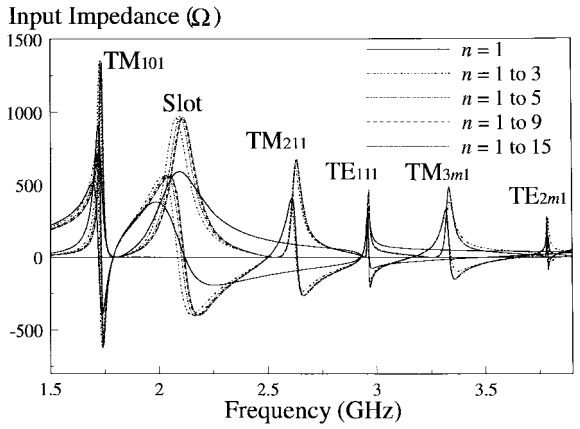

Fig. 2. Convergence check for the modal solution G_H: $L = 7.0$ cm, $W = 2.0$ mm, $a = 7.28$ cm, $x_d = 6.0$ cm, and $y_d = 0.0$ cm.

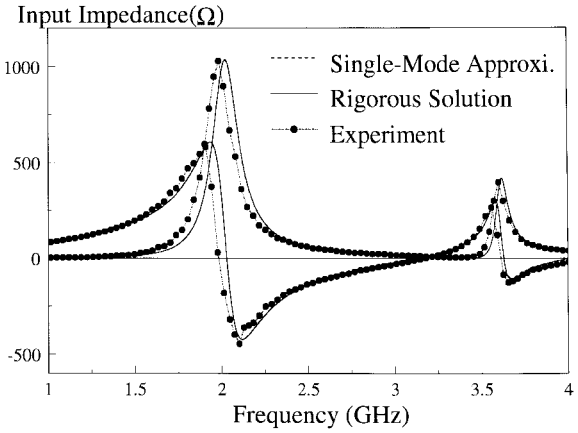

Fig. 3. Measured and calculated input impedance against frequency for $a = 6.25$ cm: $L = 7.0$ cm, $W = 2.0$ mm, $x_d = 0.0$ cm, and $y_d = 0.0$ cm.

used in the convergence check. The check is shown in Fig. 2, where it is found that using nine modal terms is good enough for the current antenna parameters.

With reference to Fig. 2, several resonances are excited due to the slot displacement x_d. Their resonance modes are labeled in the figure. For the slot resonance, the calculated resonant frequency (zero reactance) is 2.12 GHz, which is 5% higher than the value of 2.02 GHz obtained from the MoM solution of the open slot. As the cavity alters the slot's energy distribution, the difference between the cavity-backed and open-slot results is expected. It is worth mentioning that the cavity resonances at zero reactance are not caused by the cavity alone but also by the slot, i.e., they are forced resonances. To determine the resonances caused solely by the cavity, one should look for the natural resonances, which occur at the minimum resistance points [7]. At the natural resonances of a spherical cavity, the tangential electric field on the equatorial plane $(z = 0)$ is zero (or becomes extremely weak in the slot region due to the presence of the slot). This is, in fact, the reason why the presence of the ground plane cannot eliminate the modes. The vanishingly small electric field in the slot weakens the coupling between the slot and the cavity, causing the resistance to be so small. The cavity's (natural) resonant frequencies can be predicted from their eigen values [21, p. 270]. The predicted and calculated resonant frequencies (min resistance) of the various resonant modes were compared and perfect agreement between them was found. The result using the (TE_{111}) single-mode approximation [12] was plotted in the same figure but a large discrepancy found even around the TE_{111}-mode resonance. This is because the fields inside the cavity are now strongly affected by other resonant modes, which have been neglected in the single-mode theory. Therefore, one should use the rigorous solution if the slot has a rather large offset x_d.

Fig. 3 shows the input impedance as a function of frequency for $a = 6.25$ cm. The slot is located at the center of the cavity $(x_d = y_d = 0)$. As can be observed from the figure, good agreement between theory and experiment is obtained. The error may be caused by the conductor loss which has been neglected in the present theory. Two resonances are observed; the first one is caused by the slot, while the second one by the cavity TE_{111} mode. Note that for now only M_r component

TABLE I
THE MEASURED AND CALCULATED RESONANT FREQUENCIES FOR $a = 6.25, 7.28$, AND 8.73 CM. OTHER PARAMETERS ARE THE SAME AS FIG. 3. (a) THE SLOT RESONANCE. (b) THE CAVITY RESONANCE

Radius	Slot f_r (zero reactance) (GHz)		
a (cm)	Calculated	Measured	error (%)
6.25	2.03	1.99	2.01
7.28	1.99	1.97	1.02
8.73	1.94	1.92	1.04

(a)

Radius	Cavity f_r (min. resistance) (GHz)			Cavity f_r (zero reactance) (GHz)		
a (cm)	Calculated	Measured	error (%)	Calculated	Measured	error (%)
6.25	3.43	3.38	1.48	3.63	3.61	0.55
7.28	2.95	2.95	0.00	3.12	3.12	0.00
8.73	2.46	2.45	0.41	2.63	2.64	0.38

(b)

exists; all TM modes disappear, as expected. Moreover, the degenerate TE_{201} and TE_{221} modes also disappear at this particular slot position. Two other cases of $a = 7.28$ and 8.73 cm were calculated and measured. It was found that the cavity radius a mainly affects the cavity resonance, as expected; the larger the radius a, the lower the cavity resonant frequency and the higher the cavity peak resistance. Table I(a) lists the measured and calculated resonant frequencies of the slot resonance for the three cases and very good agreements are obtained. From the table, it is found that the resonant frequency shifts downward slightly for a larger cavity, which is consistent with the fact that an antenna of larger size has a lower resonant frequency. Table I(b) gives the measured and calculated resonant frequencies of the cavity resonances. Both the natural (min resistance) and forced (zero reactance) resonances are considered. Note that their resonant frequencies are decreased with increasing a, which is to be expected. The natural resonant frequencies were predicted using $k_0 a = 4.493$ and the results were in perfect agreement with the calculated values. For ease of comparison, the single-mode result is also plotted in Fig. 3. Observe that the single-mode result is so accurate that it coincides with that using the rigorous

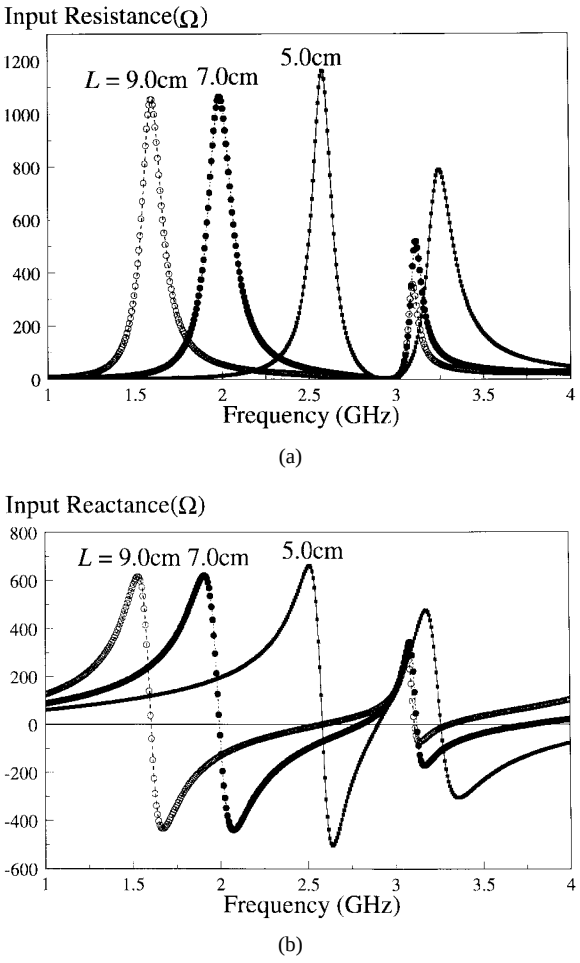

Fig. 4. Calculated input impedance against frequency for $L = 5.0, 7.0,$ and 9.0 cm: $W = 2.0$ mm, $a = 7.28$ cm, $x_d = 0.0$ cm, and $y_d = 0.0$ cm. (a) Input resistance. (b) Input reactance. Lines: rigorous solution. Dots: single-mode approximation.

solution, showing an extremely fast convergence of G_H when $x_d = y_d = 0$. This allows one to use the single-mode approximation in the antenna design for this particular slot location.

Fig. 4(a) and (b) shows the calculated input resistance and reactance, respectively, of the antenna configuration for $L = 5.0, 7.0, 9.0$ cm with $a = 7.28$ cm and $x_d = y_d = 0$. Measurements were done to verify the calculations and good agreements between them were found. However, for clarity only the calculated results are shown in the figures. With reference to the figures for both the slot and cavity resonances, the peak impedances and resonant frequencies increase with decreasing L. It was found that the slot length L has a larger influence on the slot resonance than on the cavity, as expected. The single-mode results are also shown in the same figures for easy comparison and they agree very well with the rigorous results. This shows that the accuracy of the single-mode theory depends on the slot location rather than the cavity size or the slot length.

The measured and calculated input resistance with $y_d = 3.0$ cm is shown in Fig. 5. With reference to the figure, the offset y_d retrieves the degenerate cavity TE_{201} and TE_{221} modes. From the theory, the resonant frequency (min. resistance) of

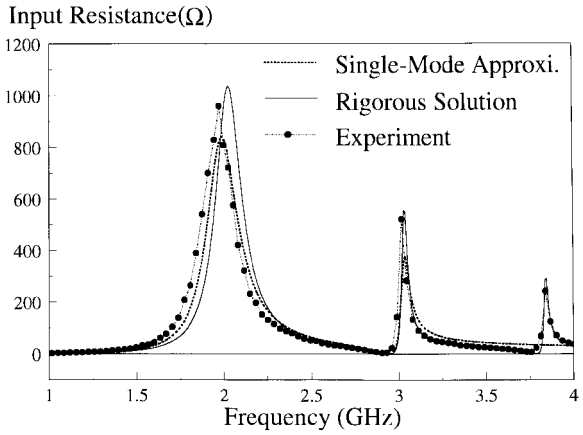

Fig. 5. Measured and calculated input resistance against frequency with an slot offset $y_d = 3$ cm: $L = 7.0$ cm, $W = 2.0$ mm, $a = 7.28$ cm, and $x_d = 0.0$ cm.

the degenerate TE_{201} and TE_{221} modes is 3.78 GHz, which is very close to the measured value of 3.75 GHz (0.8% error). These values agree very well with the predicted value of 3.78 GHz using $k_0 a = 5.76$. For ease of comparison, the single-mode result is also shown in the same figure. Note that the single-mode theory does not account for the degenerate TE_{201} and TE_{221} modes, as expected. Moreover, the single-mode theory is less accurate than the rigorous solution. Therefore, if the slot has an offset $y_d \neq 0$, one should use the rigorous solution for accurate results.

Fig. 6(a) shows the magnitude of the magnetic current (or the aperture E-field) in the slot around the slot resonance. Due to symmetry of the current, only the positive half $(0 \leq y \leq L/2)$ is shown. As can be observed from the figure, the current has the largest amplitude at the slot resonance ($f = 1.99$ GHz) as expected. The amplitude is decreased significantly at $f = 1.69$ and 2.29 GHz (± 0.3 GHz beyond the resonance) and further decreased at $f = 1.39$ and 2.59 GHz (± 0.6 GHz beyond the resonance). The inset of the figure shows the normalized magnetic current. With reference to the inset, the current shows a $\lambda/4$ waveform at the resonant frequency (1.99 GHz), as expected. The normalized current waveform is stretched up and down at the higher and lower frequencies, respectively. Fig. 6(b) shows the magnitude of the magnetic current in the slot around the cavity resonance. Like the slot-resonance case, the magnetic current is strongest at the resonant frequency (zero reactance) of 3.12 GHz, beyond which the amplitude of the current becomes smaller. It is interesting to note that at the natural resonance ($f = 2.95$ GHz), the amplitude of the magnetic current is relatively small. The normalized magnetic current is shown in the inset, where it is observed that the trend of the current is similar to that of the slot-resonance case.

Fig. 7 shows the phases of the magnetic currents of Fig. 6 at $f = 1.99, 2.95,$ and 3.12 GHz. With reference to the figure, the phases are zero at $y = 0$ for $f = 1.99$ GHz (slot resonance) and $f = 3.12$ GHz (cavity forced resonance), causing the input impedance to be purely real at these frequencies. The phases are decreased gradually along the slot. On the other hand, the phase of the current is 90° at $y = 0$ for $f = 2.95$ GHz (slot

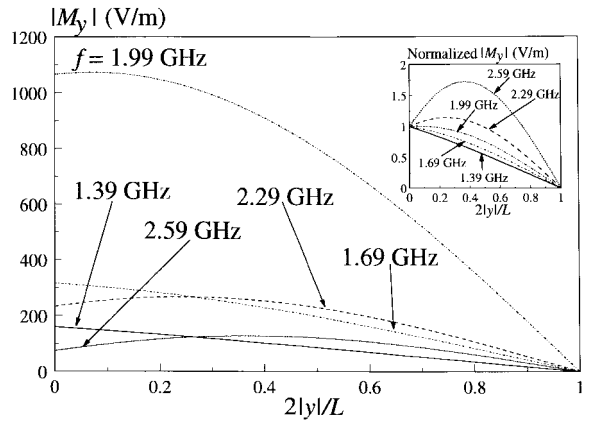

(a)

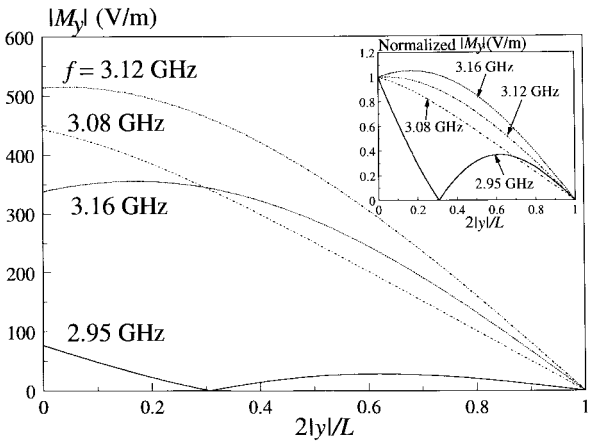

(b)

Fig. 6. Calculated magnitude of the equivalent magnetic current in the slot for $a = 7.28$ cm. Other parameters are the same as Fig. 3. (a) Around the slot resonance. (b) Around the cavity resonance.

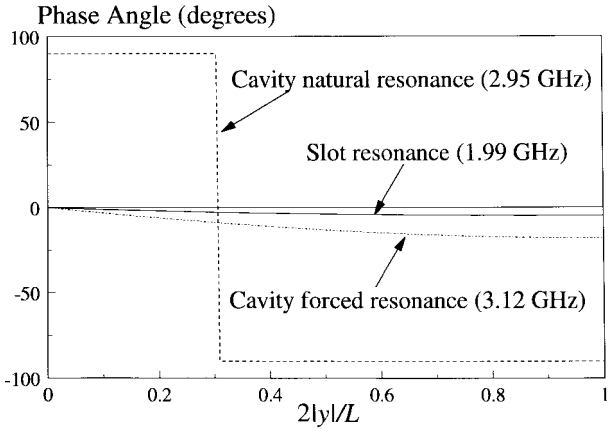

Fig. 7. Calculated phase of the equivalent magnetic current of Fig. 6 at the slot resonance and at the cavity natural and forced resonances.

natural resonance). This implies that, at this frequency, the energy of the antenna is reactive and cannot be radiated, as is reflected in the fact that the input resistance is almost zero at this frequency. It is interesting to note that there is a 180° phase change at $2|y|/L = 0.31$, hence, forming two parts of the current (totally three parts for the whole slot) which are of opposite directions. Unlike the other two cases ($f = 1.99$ and 3.12 GHz) in which the magnetic currents are able to radiate energy, the magnetic current at $f = 2.95$ GHz cannot have a net radiation as the far fields radiated by the antiphase currents are canceled out.

VI. Conclusion

The input impedance of the hemispherical cavity-backed slot antenna has been studied theoretically and experimentally. The Green's function technique together with the method of moments have been used to solve the problem. The first few fundamental TE and TM modes of the cavity have been found and their excitation discussed. Furthermore, discussions on the forced and natural resonances of the cavity have been addressed. The effects of the cavity size, the slot length, and the slot offset on the input impedance have been studied, and very good agreement between theory and experiment has been obtained. Furthermore, the variations of the magnetic current around the slot and cavity resonances have been discussed.

The convergence of the modal solution has been investigated. Moreover, the present rigorous theory has been compared with the (TE_{111}) single-mode theory. The latter is accurate only when the slot is located at the center of the cavity, where the TE_{111} mode is strongly excited. At other slot locations, the fields inside the cavity are severely affected by other resonant modes and the rigorous theory should be used instead. The result is similar to that previously found for the hemispherical dielectric resonator antenna [14].

Acknowledgment

The authors would like to thank Prof. K. K. Mei for his valuable discussions. One of the authors, K. W. Leung, would like to thank Prof. K. M. Luk for his patient guidance during the study of electromagnetic theory.

References

[1] H. G. Booker, "Slot aerials and their relation to complementary wire aerials (Babinet's principle)," *J. Inst. Elec. Eng.*, vol. III-A, pp. 620–626, 1946.

[2] C. R. Cockrell, "The input admittance of the rectangular cavity-backed slot antenna," *IEEE Trans. Antennas Propagat.*, vol. AP-24, pp. 228–294, May 1976.

[3] J. Galejs, "Admittance of a rectangular slot which is backed by a rectangular cavity," *IEEE Trans. Antennas Propagat.*, vol. AP-11, pp. 119–126, Mar. 1963.

[4] A. Hadidi and M. Hamid, "Aperture field and circuit parameters of cavity-backed slot radiator," *Proc. Inst. Elect. Eng.*, vol. 136, pt. H, pp. 139–146, Apr. 1989.

[5] S. A. Long, "Experimental study of the impedance of cavity-backed slot antennas," *IEEE Trans. Antennas Propagat.*, vol. AP-23, pp. 1–7, Jan. 1975.

[6] ———, "A mathematical model for the impedance of the cavity-backed slot antenna," *IEEE Trans. Antennas Propagat.*, vol. AP-25, pp. 829–833, Nov. 1977.

[7] E. M. Biebl and G. L. Friedsam, "Cavity-backed aperture antennas with dielectric and magnetic overlay," *IEEE Trans. Antennas Propagat.*, vol. 43, pp. 1226–1232, Nov. 1995.

[8] M. Li, K. A. Hummer, and K. Chang, "Theoretical and experimental study of the input impedance of the cylindrical cavity-backed rectangular slot antennas," *IEEE Trans. Antennas Propagat.*, vol. 39, pp. 1158–1166, Aug. 1991.

[9] D. R. Rhodes, "On the stored energy of planar apertures," *IEEE Trans. Antennas Propagat.*, vol. 14, pp. 676–683, Nov. 1966.

[10] W. A. Imbriale and P. G. Ingerson, "On numerical convergence of moment solutions of moderately thick wire antennas using sinusoidal

basis functions," *IEEE Trans. Antennas Propagat.*, vol. AP-21, pp. 363–366, May 1973.
[11] K. W. Leung, "Rigorous analysis of dielectric resonator antenna using the method of moments," Ph.D. dissertation, Chinese Univ. Hong Kong, May 1993.
[12] K. W. Leung and K. Y. Chow, "Analysis of the hemispherical cavity-backed slot antenna," *Electron. Lett.*, vol. 32, pp. 1430–1431, Aug. 1996.
[13] K. W. Leung, K. M. Luk, K. Y. A. Lai, and D. Lin, "Input impedance of dielectric resonator antenna," *Electron. Lett.*, vol. 27, pp. 2259–2260, Nov. 1991.
[14] K. M. Luk, K. W. Leung, and S. M. Shum, "Numerical study of dielectric resonator antenna," *Advances in Microstrip and Printed Antenna*, K. F. Lee and W. Chen, Eds. New York: Wiley, 1997, ch. 11, pp. 553–592.
[15] K. W. Leung, K. Y. A. Lai, K. M. Luk, and D. Lin, "Input impedance of aperture coupled hemispherical DR antenna," *Electron. Lett.*, vol. 29, pp. 1165–1167, June 1993.
[16] K. W. Leung, K. M. Luk, K. Y. A. Lai, and D. Lin, "On the TM_{101} mode of dielectric resonator antenna," *Microwave Opt. Technol. Lett.*, vol. 6, no. 11, pp. 626–629, Sept. 1993.
[17] ———, "Theory and experiment of probe-fed dielectric resonator antenna," *IEEE Trans. Antennas Propagat.*, vol. 41, pp. 1390–1398, Oct. 1993.
[18] R. D. Nevels, "The annular aperture antenna with a hemispherical center conductor extension," *IEEE Trans. Antennas Propagat.*, vol. AP-35, pp. 41–45, Jan. 1987.
[19] R. W. P. King, *Theory of Linear Antennas*. Cambridge, MA: Harvard Univ. Press, 1956, pp. 16–20.
[20] J. D. Kraus, *Antennas*, 2nd ed. New York: McGraw-Hill, 1988, pp. 391–392.
[21] R. F. Harrington, *Time Harmonic Electromagnetic Fields*. New York: McGraw-Hill, 1961.
[22] K. W. Leung, K. M. Luk, K. Y. A. Lai, and D. Lin, "Theory and experiment of an aperture-coupled hemispherical dielectric resonator antenna," *IEEE Trans. Antennas Propagat.*, vol. 43, pp. 1192–1198, Nov. 1995.
[23] R. E. Collin and F. J. Zucker, *Antenna Theory*. New York: McGraw-Hill, 1961, p. 55.

K. W. Leung (S'90–M'93), for a photograph and biography, see p. 1198 of the November 1995 issue of this TRANSACTIONS.

K. Y. Chow was born in Guangdong Province, China, in 1971. He received the B.Eng. degree in electronic engineering from the City University of Hong Kong, in 1995. He is currently working toward the Ph.D. degree in the Department of Electronic Engineering, City University of Hong Kong.

His research interests include the dielectric resonator antennas, cavity-backed slot antennas, and antenna arrays.